

TinyAlign: Boosting Lightweight Vision-Language Models by Mitigating Modal Alignment Bottlenecks

Yuanze Hu¹ Zhaoxin Fan^{1,2*} Xinyu Wang¹ Gen Li¹ Ye Qiu¹ Zhichao Yang¹

Wenjun Wu^{1,2}

Kejian Wu³

Yifan Sun⁴

Xiaotie Deng⁵

Jin Dong⁶

¹ Beijing Advanced Innovation Center for Future Blockchain and Privacy Computing, Beihang University ² Hangzhou International Innovation Institute, Beihang University

³ Xreal, ⁴ Renmin University, ⁵ Peking University

⁶ Beijing Academy of Blockchain and Edge Computing (BABEC)

Abstract

Lightweight Vision-Language Models (VLMs) are indispensable for resource-constrained applications. The prevailing approach to aligning vision and language models involves freezing both the vision encoder and the language model while training small connector modules. However, this strategy heavily depends on the intrinsic capabilities of the language model, which can be suboptimal for lightweight models with limited representational capacity. In this work, we investigate this alignment bottleneck through the lens of mutual information, demonstrating that the constrained capacity of the language model inherently limits the Effective Mutual Information (EMI) between multimodal inputs and outputs, thereby compromising alignment quality. To address this challenge, we propose TinyAlign, a novel framework inspired by Retrieval-Augmented Generation, which strategically retrieves relevant context from a memory bank to enrich multimodal inputs and enhance their alignment. Extensive empirical evaluations reveal that TinyAlign significantly reduces training loss, accelerates convergence, and enhances task performance. Remarkably, it allows models to achieve baseline-level performance with only 40% of the fine-tuning data, highlighting exceptional data efficiency. Our work thus offers a practical pathway for developing more capable lightweight VLMs while introducing a fresh theoretical lens to better understand and address alignment bottlenecks in constrained multimodal systems.

1 Introduction

The rapid advancements in Large Language Models (LLMs) have catalyzed the development of Vision-Language Models (VLMs), enabling models to excel in complex multimodal reasoning and understanding tasks. Prominent models such as Gemini 2.5 Pro [12], GPT-4V [29], Qwen2.5-VL 72B [2], and PaLI-X [6] have showcased remarkable performance across various benchmarks, setting new standards for multimodal intelligence. However, these models typically involve billions of parameters, resulting in significant computational and storage demands. Such massive requirements make these models impractical for resource-constrained scenarios, such as edge devices or applications with limited computational budgets. This growing demand for efficiency has turned lightweight VLMs

*Corresponding author

into a critical area of research, as they aim to retain strong multimodal capabilities while drastically reducing computational costs and memory footprints, thereby enabling broader applicability.

To achieve this balance between performance and efficiency, most VLMs adopt a modular design where pre-trained vision encoders and language models are frozen, and a small "connector" module is trained to align the two modalities. This approach, also seen in lightweight models such as MiniGPT-4 [46], BLIP-2 [20], and Visual Instruction Tuning [23], is computationally efficient and leverages the strong representational power of pre-trained components. However, while effective, this implicit alignment paradigm might struggle in the context of lightweight VLMs. The limited representational capacity of smaller LLMs significantly constrains their ability to process and align multimodal information, leading to subpar performance on complex tasks. This misalignment becomes a critical bottleneck for lightweight VLMs, as it prevents these models from fully realizing their potential.

To address this issue, we conduct a theoretical analysis of the alignment bottleneck in lightweight VLMs from the perspective of information theory [47, 24]. Specifically, we introduce the concept of Effective Mutual Information (EMI) to quantify the amount of information a model can practically leverage given its capacity constraints. Our analysis reveals that freezing the parameters of a lightweight language model inherently limits the EMI, creating a bottleneck that restricts the model’s ability to align multimodal inputs effectively. This limitation manifests in suboptimal learning dynamics when using standard training objectives, such as cross-entropy loss, and highlights the need for new strategies to enhance the effective flow of information during alignment.

Motivated by this insight, we propose TinyAlign, a novel pre-training and fine-tuning framework explicitly designed to overcome this alignment bottleneck. Inspired by Retrieval-Augmented Generation (RAGs) [19, 14, 15], TinyAlign introduces a memory bank constructed from multimodal training instances within the dataset, setting it apart from traditional approaches that depend on external knowledge sources. During training, the framework retrieves contextually relevant representations from the memory bank and augments the original visual inputs with enriched multimodal context. By increasing the effective information content available to the model, TinyAlign reduces the inherent learning difficulty posed by the limited capacity of lightweight language models. This design not only enhances alignment but also optimizes the utilization of available training data, addressing the core challenges faced by lightweight VLMs.

We validate the effectiveness of TinyAlign through extensive experiments across a diverse set of lightweight architectures, including Vicuna [8], Phi-2 [13], TinyLLaMA [44], and Qwen2 [36], as well as vision encoders like SigLIP [43] and CLIP [30]. Our results demonstrate that TinyAlign significantly accelerates convergence, reduces alignment losses (Fig. 1(a)), and produces more compact and meaningful feature representations (Fig. 1(b)). Furthermore, TinyAlign exhibits exceptional data efficiency, achieving baseline-level performance with only 40% of the fine-tuning data. Our contribution can be summarized as:

- We identify a fundamental alignment bottleneck in lightweight VLMs, theoretically analyzing its root cause using principles from information theory. Our analysis reveals that the limited capacity of lightweight LLMs constrains the effective information flow during multimodal alignment.
- We propose TinyAlign, a novel framework inspired by Retrieval-Augmented Generation, which enriches multimodal inputs by retrieving relevant context from a memory bank. This approach enhances the effective information content accessible to the model, addressing the alignment bottleneck.
- We conduct extensive experiments to validate the effectiveness of TinyAlign, demonstrating notable improvements in convergence speed, alignment quality, downstream task performance, and data efficiency compared to conventional alignment methods.

2 Related Work

The LLM-Centric Paradigm in VLMs. The LLM-Centric Paradigm has become a dominant framework in Vision-Language Models, leveraging pre-trained Large Language Models as the core for cross-modal understanding [36, 2, 25, 20, 4, 7]. This approach typically freezes the parameters of both the vision encoder and the LLM [20], while training a lightweight connector module to bridge vision and language [36]. This implicit alignment strategy has achieved notable empirical success, as

seen in models like DeepSeek-VL [25] and Qwen2.5-VL [2]. However, the theoretical mechanisms enabling effective cross-modal harmonization remain underexplored, with most research focusing on empirical results rather than systematic analysis. To fill this gap, our work conducts one of the first in-depth theoretical investigations into this paradigm, uncovering its principles and limitations to better understand cross-modal alignment.

Advancements in Lightweight VLMs. Recent efforts to create lightweight Vision-Language Models (VLMs) have explored various avenues for enhancing efficiency and performance [41, 45, 39, 27, 33]. EfficientVLM [35] introduces a distill-then-prune framework with modal-adaptive pruning to compress large VLMs effectively. TinyLLaVA [45] explores optimal pairings of language models, vision encoders, and connectors for small-scale VLMs, while MobileVLM and its successor v2 emphasize architectural innovations, high-quality data, and advanced training strategies [9, 10], while SmolVLM [27] further explores tokenization strategies. MiniCPM-V [39] presents a series of efficient Multimodal Large Language Models (MLLMs) designed for on-device deployment, achieved by integrating advanced techniques in architecture, pre-training, and alignment. However, these approaches primarily focus on component optimization, model compression, advanced training strategies, or designing for edge deployment, and seldom question whether the widely adopted implicit alignment paradigm is fundamentally suitable for models with limited capacity. In contrast, we provide a principled analysis demonstrating that this paradigm intrinsically induces higher alignment loss for smaller models, thereby limiting their potential for robust visual understanding and cross-modal alignment.

Retrieval-Augmented Models. Retrieval-Augmented Generation enhances factual accuracy in NLP by integrating external knowledge retrieval with parametric models [19]. Techniques like unsupervised retriever pre-training enable efficient access to large-scale documents during training and inference [14]. RAG now extends to multimodal tasks, with MM-REACT combining language models and vision experts for complex reasoning [37], and Re-ViLM reducing parameters by storing knowledge externally for image-to-text generation [38]. Frameworks like RAVEN and MuRAG apply retrieval for multitask learning and open-domain question answering [31, 5], while models like REVEAL unify memory, retrieval, and generation across diverse sources [15]. These approaches rely on large external memory banks and retriever modules to broaden knowledge for reasoning-heavy tasks [3, 15, 31]. In contrast, TinyAlign addresses the EMI bottleneck in lightweight VLMs by constructing a memory bank from multimodal *training instances*. During pre-training and fine-tuning, TinyAlign retrieves relevant representations to augment visual input, increasing mutual information between inputs and outputs and overcoming the limitations of compact models.

3 Theoretical Framework: LLM-Centric Alignment and Its Limitations

3.1 Cross-Entropy Loss in LLM-Centric VLM Pre-training

We begin with an analysis of the commonly used LLM-centric paradigm for Vision-Language Models, where the objective is to align visual information with a pre-trained LLM. In this setup, the visual input is denoted as X_V , the accompanying textual instruction as X_I , and the target output, often a textual description or answer, as L .

The processing pipeline in this paradigm is structured as follows:

1. A frozen Vision Encoder (e.g., a Vision Transformer, ViT) with parameters θ_{ViT} processes the visual input X_V to extract visual features: $Z_V = ViT(X_V; \theta_{ViT})$.
2. A trainable Connector module, parameterized by θ_C^* , transforms the visual features Z_V into embeddings H_V compatible with the LLM’s input space: $H_V = Connector(Z_V; \theta_C^*)$.
3. Simultaneously, the textual instruction X_I is processed by the frozen LLM’s input embedding layer (parameterized by θ_{LLM}), generating instruction embeddings: $H_I = LLM_{embed}(X_I; \theta_{LLM})$.
4. The visual embeddings H_V and instruction embeddings H_I are concatenated to form the joint input: $H_{in} = [H_V, H_I]$.
5. Finally, the frozen LLM produces an output distribution over the target L : $P_{model}(L|H_{in}; \theta_{LLM})$.

3.2 The LLM Bottleneck: Irreducible Error and Effective Mutual Information

As discussed before, we believe the LLM-centric paradigm inherently suffers from a bottleneck due to its reliance on implicit alignment mechanisms. To understand this limitation, we analyze it from an information-theoretic perspective and show how it constrains the system’s ability to fully utilize the information in the inputs. The starting point of this analysis is the conditional cross-entropy (CE) loss, which measures the discrepancy between the true conditional distribution of the target labels L and the model’s predictions. This loss can be decomposed as follows:

$$\mathcal{L}_{\text{CE}}(\theta_C^*|X_V, X_I) = H(P_{\text{true}}(L|X_V, X_I)) + D_{\text{KL}}(P_{\text{true}}(L|X_V, X_I) || P_{\text{model}}(L|[H_V(\theta_C^*), H_I]; \theta_{\text{LLM}})) \quad (1)$$

Here, $H(P_{\text{true}}(L|X_V, X_I))$ represents the true conditional entropy of L given the inputs (X_V, X_I) , which is independent of the model parameters and reflects the irreducible uncertainty in the labels. The second term, the KL divergence, measures the gap between the true conditional distribution and the model’s predictions. Thus, minimizing $\mathcal{L}_{\text{CE}}(\theta_C^*)$ is equivalent to minimizing the KL divergence term, as the conditional entropy is fixed.

At the beginning of training, the Connector parameters θ_C^* are randomly initialized, leading to arbitrary and semantically meaningless visual embeddings $H_V(\theta_C^*)$ from the perspective of the frozen LLM (θ_{LLM}). When the LLM processes these unfamiliar embeddings H_V alongside H_I , it produces outputs that deviate significantly from the true target L , resulting in a high initial loss. During training, the Connector learns to transform raw visual features Z_V into embeddings H_V that the frozen LLM can interpret coherently with H_I to predict L . This process can be viewed as the Connector "translating" visual information into the LLM’s fixed semantic space. However, even with an optimal Connector θ_C^{opt} that produces the best possible H_V , the frozen LLM’s representational capacity is inherently limited. Its ability to integrate and reason over the novel visual embeddings H_V is constrained by its fixed architecture and pre-trained knowledge. This introduces an irreducible error, quantified as the average KL divergence that cannot be eliminated even with optimal Connector parameters:

$$\bar{\epsilon}_{\theta_{\text{LLM}}} = \mathbb{E}_{(X_V, X_I)} \left[\min_{\theta_C^*} D_{\text{KL}}(P_{\text{true}}(L|X_V, X_I) || P_{\text{model}}(L|[\text{Connector}(Z_V; \theta_C^*), H_I]; \theta_{\text{LLM}})) \right] \geq 0$$

This irreducible error, $\bar{\epsilon}_{\theta_{\text{LLM}}}$, reflects the frozen LLM’s inability to fully align its semantic space with the optimally transformed visual embeddings H_V . The minimum achievable CE loss for the system, given the frozen parameters θ_{vIT} and θ_{LLM} , can therefore be expressed as:

$$\min_{\theta_C^*} \mathcal{L}_{\text{CE}}(\theta_C^*) = H(L|X_V, X_I) + \bar{\epsilon}_{\theta_{\text{LLM}}} \quad (2)$$

Here, $H(L|X_V, X_I)$ represents the irreducible uncertainty in the target labels, while $\bar{\epsilon}_{\theta_{\text{LLM}}}$ quantifies the frozen LLM’s limitations. To further analyze this bottleneck, we rewrite the minimum loss using the definition of mutual information $I(X; Y) = H(Y) - H(Y|X)$. Substituting $H(L|X_V, X_I)$ into Eq. (2), we obtain:

$$\min_{\theta_C^*} \mathcal{L}_{\text{CE}}(\theta_C^*) = H(L) - I(X_V, X_I; L) + \bar{\epsilon}_{\theta_{\text{LLM}}} \quad (3)$$

Here, $H(L)$ is the entropy of the target labels, and $I(X_V, X_I; L)$ is the true mutual information between the inputs (X_V, X_I) and the labels L . To capture the system’s actual capability to utilize information, we define an "Effective Mutual Information" (I_{eff}), which represents the mutual information the system can effectively leverage, accounting for the irreducible error $\bar{\epsilon}_{\theta_{\text{LLM}}}$:

$$I_{\text{eff}}(X_V, X_I; L | \theta_{\text{LLM}}, \theta_{\text{vIT}}) = I(X_V, X_I; L) - \bar{\epsilon}_{\theta_{\text{LLM}}} \quad (4)$$

Substituting I_{eff} into Eq. (3), the minimum achievable loss becomes:

$$\min_{\theta_C^*} \mathcal{L}_{\text{CE}}(\theta_C^*) \approx H(L) - I_{\text{eff}}(X_V, X_I; L | \theta_{\text{LLM}}, \theta_{\text{vIT}}) \quad (5)$$

This result highlights a critical limitation of the LLM-centric paradigm: the effective mutual information (I_{eff}) is fundamentally constrained by the frozen LLM’s ability to process and integrate visual embeddings. Even with perfect transformation of visual features by the Connector, the irreducible error $\bar{\epsilon}_{\theta_{\text{LLM}}}$ reduces the system’s ability to fully utilize the true mutual information $I(X_V, X_I; L)$. It underscores the need for alternative approaches to achieve better cross-modal alignment.

Hypothesis on LLM Scale. Based on the theoretical analysis above, we hypothesize that a smaller, lightweight LLM (with parameters $\theta_{\text{LLM,small}}$) possesses a more restricted representational capacity and is inherently less capable of interpreting and integrating novel semantic inputs H_V compared to a larger, more powerful LLM (with parameters $\theta_{\text{LLM,large}}$). As shown in Fig. 2(a), the larger LLM exhibits a low loss even before ever seeing the image, suggesting its superior capacity to handle semantic information. This implies:

$$\bar{\epsilon}_{\theta_{\text{LLM,small}}} \geq \bar{\epsilon}_{\theta_{\text{LLM,large}}}$$

Consequently, from Eq. (4), the effective mutual information for a system using a smaller LLM will be lower:

$$I_{\text{eff}}(X_V, X_I; L | \theta_{\text{LLM,small}}, \theta_{\text{ViT}}) \leq I_{\text{eff}}(X_V, X_I; L | \theta_{\text{LLM,large}}, \theta_{\text{ViT}})$$

And from Eq. (2), its minimum achievable CE loss will be higher:

$$\min_{\theta_C^*} \mathcal{L}_{\text{CE}}(\text{using } \theta_{\text{LLM,small}}) \geq \min_{\theta_C^*} \mathcal{L}_{\text{CE}}(\text{using } \theta_{\text{LLM,large}})$$

This theoretical observation explains why VLMs built upon smaller frozen LLMs often converge to higher loss values and exhibit poorer performance. The LLM’s intrinsic capacity to process and integrate the optimally transformed visual embeddings H_V becomes the bottleneck for the entire VLM’s capability.

4 TinyAlign: Mitigating Modal Alignment Bottleneck of Lightweight VLMs

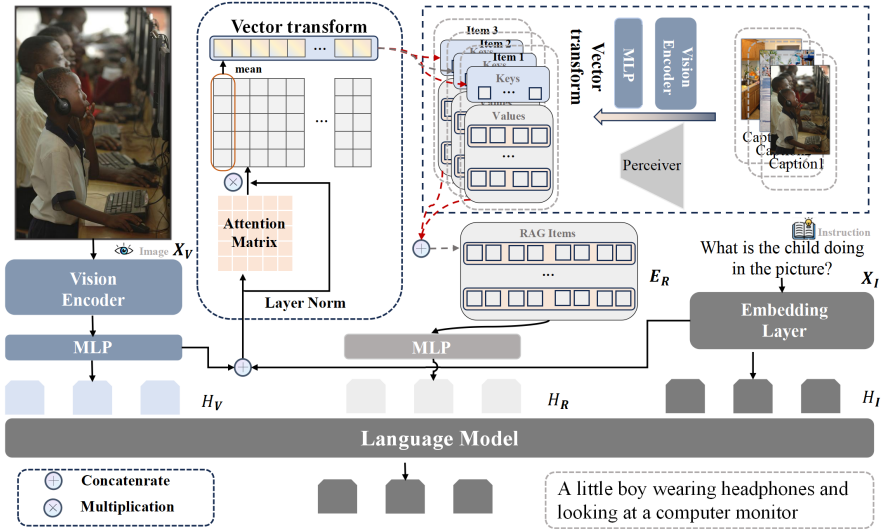


Figure 1: Architectural overview of TinyAlign. Given an input image X_V and instruction X_I , a query key derived from these inputs retrieves k similar, Perceiver-compressed multimodal embeddings $E_R = \{E_{R_j}\}_{j=1}^k$ from a pre-constructed Memory Bank. These cues E_R are processed by a trainable RAG Connector (θ_{RC}^*) into an auxiliary representation H_R . Concurrently, X_V is processed by a Vision Transformer (ViT) and a primary Connector (θ_C^*) into visual features H_V . The instruction X_I is embedded as H_I . Finally, a frozen LLM receives the composite input $H'_{\text{in}} = [H_V, H_R, H_I]$ for prediction. This architecture enhances lightweight VLMs by supplying efficiently processed, relevant contextual information, thereby alleviating the LLM’s processing burden.

4.1 Theoretical Analysis: Enhancing Effective Mutual Information via RAG

Lightweight, frozen LLMs ($\theta_{\text{LLM,small}}$) often exhibit high irreducible error $\bar{\epsilon}_{\theta_{\text{LLM}}}$. TinyAlign (Fig. 1), a Retrieval-Augmented Generation (RAG)-enhanced connector architecture, mitigates this by boosting

effective mutual information (I_{eff}) with strategically compressed, relevant contextual cues, thereby reducing the LLM’s intrinsic processing demands.

A standard VLM maps visual input X_V (via ViT θ_{ViT} and primary connector θ_C^*) to H_V , with instruction embeddings H_I . TinyAlign augments this by: 1) retrieving k pre-compressed embeddings E_R from a memory bank \mathcal{M} (Sec. 4.2); 2) employing a trainable RAG connector (θ_{RC}^*) to transform E_R into supplementary representations H_R ; and 3) presenting a composite input $H'_{\text{in}} = [H_V, H_R, H_I]$ to the frozen LLM. Trainable parameters are $\Theta_C^* = \{\theta_C^*, \theta_{RC}^*\}$. We posit that incorporating E_R (forming augmented context $X' = (X_V, E_R, X_I)$) enhances I_{eff} . The change, ΔI_{eff} , is:

$$\begin{aligned} \Delta I_{\text{eff}} &= [I(X'; L) - \bar{\epsilon}_{\theta_{\text{LLM}}}(X')] - [I(X_V, X_I; L) - \bar{\epsilon}_{\theta_{\text{LLM}}}(X_V, X_I)] \\ &= \underbrace{I(E_R; L|X_V, X_I)}_{\Delta I_{\text{true}}} + \underbrace{(\bar{\epsilon}_{\theta_{\text{LLM}}}(X_V, X_I) - \bar{\epsilon}_{\theta_{\text{LLM}}}(X'))}_{\Delta \bar{\epsilon}_{\theta_{\text{LLM}}}} \end{aligned} \quad (6)$$

$\Delta I_{\text{true}} > 0$ as E_R (from pertinent captions) provides novel information about target L . $\Delta \bar{\epsilon}_{\theta_{\text{LLM}}} > 0$ signifies reduced LLM irreducible error. The RAG connector θ_{RC}^* transforms E_R into ‘LLM-assimilable contextual hints’ from pre-compressed image-text pairs (θ_P -processed), making H'_{in} more ‘input-friendly’. This enables the fixed-capacity LLM to better approximate $P_{\text{true}}(L|X')$, reducing misinterpretations ($\bar{\epsilon}_{\theta_{\text{LLM}}}(X') < \bar{\epsilon}_{\theta_{\text{LLM}}}(X_V, X_I)$) and alleviating cognitive load, corroborated by faster convergence (Fig. 2(a)). For more theoretical details on introducing RAG to enhance effective mutual information, please refer to Appendix A.

This $\Delta \bar{\epsilon}_{\theta_{\text{LLM}}}$ reduction is crucial for lightweight VLMs with high baseline error. TinyAlign’s architecture (LLM-independent, Perceiver-based pre-compression and efficient RAG connector) maximizes this reduction, acting as a ‘cognitive scaffold’ and lowering the reasoning threshold. Consequently, when $\Delta I_{\text{eff}} > 0$ (driven by $\Delta I_{\text{true}} > 0$ and substantial $\Delta \bar{\epsilon}_{\theta_{\text{LLM}}} > 0$), the minimum achievable CE loss is reduced: $\min_{\theta_C^*} \mathcal{L}_{\text{CE}}(\text{RAG-enhanced}) < \min_{\theta_C^*} \mathcal{L}_{\text{CE}}(\text{standard})$. RAG-enhanced connectors elevate VLM performance by mitigating the burden on frozen (especially lightweight) LLMs using pre-compressed cues, increasing leverageable information despite fixed LLM capacity.

4.2 Memory Bank Design for Lightweight Efficiency

TinyAlign’s memory bank \mathcal{M} supports lightweight VLMs by storing extensive multimodal information as compact key-value (K_m, V_m) pairs from a large-scale pre-training dataset, prioritizing minimal storage and low retrieval latency, and we sample 100K image-text pairs from pre-training dataset declared in Sec. 5.1.

Key Generation. Each key $K_m \in \mathbb{R}^{d_k}$ constitutes a compact, low-dimensional embedding derived from a source image-text pair (X_{V_m}, X_{I_m}) . Its generation employs an attention-based aggregation mechanism. Specifically, multi-modal input features first pass through a self-attention layer to yield an attention matrix, capturing contextual dependencies within the inputs. These original features are then element-wise modulated by this attention matrix. Subsequently, the resultant attention-weighted features are subjected to a mean pooling operation across the token dimension (‘Vector transform’ in Fig. 1), producing the distilled key vector K_m . This process is designed to distill salient cross-modal information into a dense representation, thereby facilitating efficient similarity search and establishing K_m as a unified query anchor.

Value Generation. Each value $V_m \in \mathbb{R}^{d_v}$ is the corresponding compressed latent multimodal embedding E_{R_m} . An LLM-independent Perceiver[17] model (θ_P , Table 3) pre-processes original multimodal instances $\{(X_{V_j}, \text{Cap}_j)\}$ into these values. This pre-compression optimizes for inference speed and reduced memory transfer.

This dual-compression strategy (compact keys K_m for rapid search, highly compressed values V_m for minimal overhead) is central to TinyAlign’s efficiency, providing potent contextual cues with parsimonious resource use.

4.3 Integrated Pre-training and Instruction Tuning Stages

TinyAlign employs a two-stage training strategy, with both stages using the same objective from Eq. (5): initial connector pre-training with a frozen lightweight LLM and ViT, followed by joint LLM and connector fine-tuning with a frozen ViT for task adaptation.

Pre-training Stage. Connectors θ_C^* and θ_{RC}^* are trained while the vision encoder (θ_{ViT}) and LLM ($\theta_{LLM,small}$) remain frozen. This compels connectors to optimally format retrieved E_R (forming augmented input $H'_{in} = [H_V, H_R, H_I]$) for the LLM’s extant capabilities, addressing its higher irreducible error and reducing cognitive load. This phase validates the connector’s ability to map the semantic spaces of different pre-trained models to the LLM’s semantic space.

Instruction Tuning Stage. This stage adapts the VLM to downstream tasks. The ViT (θ_{ViT}) remains frozen. Connectors (θ_C^* , θ_{RC}^*) and, critically, the lightweight LLM ($\theta_{LLM,small}$) are fine-tuned. With connectors supplying simplified, relevant input, LLM fine-tuning enables specialized reasoning by maximally leveraging these augmented inputs from an active memory bank \mathcal{M} . This integrated approach optimizes the LLM’s utilization of the enhanced inputs.

5 Experiments

We conduct a comprehensive suite of experiments to rigorously validate the efficacy of TinyAlign. Our evaluation is designed to: (1) assess its impact on pre-training dynamics, specifically convergence speed and loss reduction (Fig. 2(a)); (2) analyze the quality of the learned representations through UMAP visualizations (Fig. 2(b)); (3) quantify performance improvements on diverse downstream multimodal tasks post-instruction tuning, detailed in Table 1; and (4) measure gains in data efficiency during instruction tuning (Sec. 5.4, Fig. 3). A thorough analysis of data efficiency across various benchmarks can be found in Appendix E (Fig. 4). Additionally, our FLOPs analysis, detailed in Appendix D (Table 4). The extensive ablation studies validating our architectural decisions are presented in Appendix F (Tables 5, 6, and 7). These experiments empirically substantiate our theoretical derivations concerning the enhancement of Effective Mutual Information (I_{eff}).

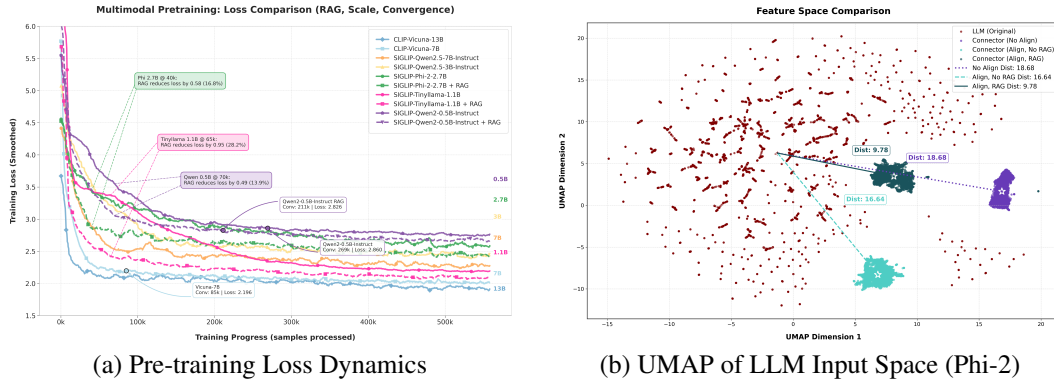


Figure 2: **(a)** Comparison of multimodal pre-training loss on the LLaVA dataset. TinyAlign-enhanced models (dashed lines, "+ RAG") exhibit accelerated convergence and lower final training loss compared to baselines (solid lines) across various model scales (e.g., 16.8% loss reduction for Phi-2.7B, 28.2% for TinyLLaMA-1.1B, 13.9% for Qwen2-0.5B at specified sample points). All models use SigLIP vision encoders, with only connector parameters trained. **(b)** UMAP visualization of the LLM (for example, Phi-2) input space for (i) baseline(dashed lines), (ii) TinyAlign-enhanced (solid lines), and (iii) a non-aligned model. TinyAlign promotes superior semantic clustering and alignment.

5.1 Experimental Setup

Our framework builds upon lightweight VLMs, drawing inspiration from TinyLLaVA [45]. We primarily utilize the LLaVA dataset family [23] for pre-training analysis and Instruction tuning, Table 2 provides details on the computational key hyperparameters used for the pre-training and Instruction tuning phases of our experiments. Detailed hyperparameter settings are available in Appendix B.

Datasets. Pre-training Data: For analyzing pre-training dynamics (Sec. 5.2) and constructing the memory bank (details in Appendix F), we employ the LLaVA pre-training set. This set comprises 558K image-text pairs from a LAION-CC-SBU subset [23], with corresponding annotations. **Instruction Tuning Data:** For evaluating instruction-following capabilities, we use the LLaVA v1.5

SFT dataset, containing approximately 665K samples. Images are sourced from diverse datasets including COCO [22], GQA [16], TextVQA [32], OCR-VQA [28], and VisualGenome [18].

Models and Baselines. We validate TinyAlign across several lightweight Large Language Models (LLMs) and vision encoders: Vicuna-7B/13B [8], Phi-2 (2.7B) [13], Gemma (2B) [34], TinyLLaMA (1.1B) [44], and Qwen2-0.5B [2]. For vision encoders, we use SigLIP [43] and CLIP [30]. Consistent with findings in TinyLLaVA [45] that favor SigLIP for lightweight VLMs, we primarily adopt SigLIP. The Connectors utilize a two-layer multilayer perceptron with GELU activation functions to transform the input features.

5.2 Pre-training Performance Analysis

Our empirical results demonstrate TinyAlign’s substantial efficacy in enhancing pre-training for lightweight Vision-Language Models (VLMs). Analysis of training loss trajectories and learned multimodal representations reveals two key benefits.

Accelerated Convergence and Reduced Training Loss. TinyAlign markedly accelerates convergence and reduces final training loss on the LLaVA pre-training dataset. As shown in Fig. 2(a), models incorporating TinyAlign, such as Phi-2 (2.7B), TinyLLaMA (1.1B), and Qwen2-0.5B, achieve significant loss reductions of 16.8%, 28.2%, and 13.9%, respectively, compared to baselines. This improved training efficiency and superior model fit empirically validate our hypothesis (Eq. (2)) that TinyAlign enhances Effective Mutual Information (I_{eff}), thereby lowering the achievable cross-entropy loss (\mathcal{L}_{CE}). These benefits are consistent across models ranging from 0.5B to 2.7B parameters, underscoring TinyAlign’s broad applicability.

Improved Embedding Space Alignment and Semantic Coherence. Qualitatively, TinyAlign cultivates superior multimodal representations. UMAP projections (Fig. 2(b)) reveal that TinyAlign (ii) produces significantly tighter, more separable, and semantically coherent image-text embedding clusters compared to the diffuse embeddings from baselines (i) and the disarray in non-aligned models (iii). This improved structural alignment, indicative of a reduced average embedding error ($\bar{\epsilon}_{\theta_{\text{LLM}}}$), is attributed to contextual cues H_R from retrieved information guiding the LLM towards more accurate inter-modal associations. Such well-structured representations are crucial for downstream task performance (see Appendix C for UMAP details).

In summary, TinyAlign demonstrably improves pre-training efficiency and yields higher-quality multimodal representations. These advancements establish a more robust foundation for downstream instruction tuning and enhanced performance across diverse VLM applications.

5.3 Instruction Tuning Performance Analysis

Post-instruction tuning, TinyAlign variants consistently outperform their respective baselines across a majority of the evaluated benchmarks, as detailed in Table 1. For instance, TinyLLaMA-1.1B equipped with TinyAlign achieves a 74.49% accuracy on VQAv2, marking a 3.51% improvement over its baseline. Similarly, Phi-2-2.7B with TinyAlign attains 78.32% on VQAv2, a 2.93% gain. These improvements generally underscore enhanced generalization capabilities stemming from superior pre-training alignment. However, on the highly complex MM-Vet benchmark, the TinyLLaMA-1.1B variant with TinyAlign exhibits a marginal performance decrease (2.4%). This suggests that for certain exceptionally challenging tasks, particularly with smaller model capacities, the benefits of alignment might be nuanced or necessitate further task-specific tuning.

5.4 Data Efficiency Analysis

TinyAlign demonstrates substantial improvements in data efficiency during instruction tuning, as depicted in Fig. 3. Our analysis reveals that TinyAlign-enhanced models (Phi-2 and TinyLLaMA) can achieve a weighted average accuracy comparable to baselines trained on 100% of the instruction tuning data while utilizing only 40% of the data. This efficiency gain is observed across various capabilities, as the Fig. 4 shows: TinyAlign significantly enhances visual reasoning (e.g., GQA, VQAv2, SQA-I), improves scene text understanding (e.g., TextVQA), and curtails model hallucinations (e.g., POPE), frequently matching or exceeding baseline performance with merely 20-60% of the data. While challenges persist for highly complex tasks such as MMMU, where gains are less uniform, the overall

Table 1: Performance comparison on various multimodal benchmarks after instruction tuning. \uparrow indicates performance improvement with TinyAlign, while \downarrow indicates a decrease.

Benchmark	TinyLLaMA-1.1B		Phi-2-2.7B		Qwen2-0.5B	
	Baseline	+TinyAlign	Baseline	+TinyAlign	Baseline	+TinyAlign
GQA [16]	52.37	56.69 \uparrow	58.44	60.73 \uparrow	56.30	57.58 \uparrow
MMM [42]	29.4	30.2 \uparrow	36.2	37.7 \uparrow	31.0	31.4 \uparrow
MM-Vet [40]	26.0	23.6 \downarrow	31.5	34.1 \uparrow	20.9	23.6 \uparrow
POPE [21]	84.3	86.0 \uparrow	86.6	88.0 \uparrow	86.4	87.2 \uparrow
SQA-I [26]	56.52	59.84 \uparrow	67.28	68.12 \uparrow	59.54	60.24 \uparrow
TextVQA [32]	46.33	46.41 \uparrow	50.31	55.48 \uparrow	46.08	46.62 \uparrow
VQAV2 [1]	70.98	74.49 \uparrow	75.39	78.32 \uparrow	72.95	74.21 \uparrow
MME [11]	1105.10	1200.67 \uparrow	1364.2	1412.1 \uparrow	1170.54	1208.87 \uparrow

results compellingly underscore TinyAlign’s capacity to facilitate the development of highly capable VLMs under data-constrained scenarios. This reduces reliance on extensive labeled datasets and can accelerate development cycles. A detailed benchmark-specific data efficiency analysis is provided in Appendix E.

5.5 Ablation Study

To systematically assess our model architecture, we conduct a series of targeted ablation studies focusing on three key design choices: (1) the size and composition of the RAG knowledge base (Memory Bank) (Table 5), (2) the design methodology for the knowledge base keys (Table 6), and (3) the number of documents (Top-K) retrieved during inference (Table 7).

The findings from these ablations, detailed in Appendix F, inform our final model configuration. We adopt a 100k-entry knowledge base, ensure alignment between the vision encoders used for VLM training and RAG key generation, and retrieve the top-5 documents to augment generation. These choices strike an optimal balance of performance, efficiency, and contextual enrichment.

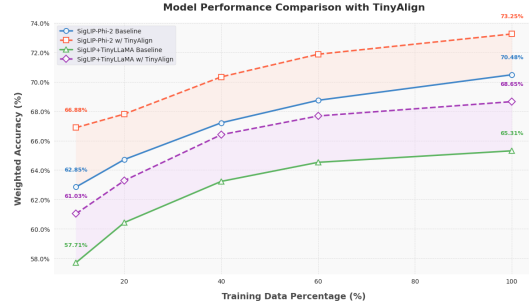


Figure 3: Model weighted accuracy, computed per Eq. (8), is evaluated against the percentage of instruction tuning data utilized. TinyAlign models consistently demonstrate superior performance, achieving higher accuracy with substantially less data relative to baseline models.

6 Discussion

Conclusion. Lightweight Vision-Language Models are essential for resource-constrained applications, yet their performance is often limited by alignment bottlenecks caused by the constrained capacity of smaller language models. Through a mutual information perspective, we demonstrate that this limitation reduces the Effective Mutual Information between multimodal inputs and outputs, compromising alignment quality. To address this, we propose TinyAlign, a framework inspired by Retrieval-Augmented Generation, which retrieves relevant context from a memory bank to enrich multimodal inputs. Empirical evaluations show that TinyAlign significantly improves task performance, reduces training loss, and accelerates convergence. Notably, it achieves baseline-level performance with only 40% of the fine-tuning data, offering a highly data-efficient solution for lightweight VLMs. This work provides both a practical framework and a theoretical foundation to address alignment challenges in constrained multimodal systems.

Limitation and Future Work. Though TinyAlign is effective, it has several limitations. Its reliance on a well-designed memory bank may require bespoke construction for different LLMs, and compatibility between the Vision Transformer or querying and memory key generation is essential.

Additionally, for challenging tasks or smaller models, further task-specific tuning may be needed. Future work could explore adaptive memory construction and more flexible ViT compatibility to enhance alignment across diverse settings.

References

- [1] Aishwarya Agrawal, Jiasen Lu, Stanislaw Antol, Margaret Mitchell, C. Lawrence Zitnick, Dhruv Batra, and Devi Parikh. Vqa: Visual question answering, 2016. URL <https://arxiv.org/abs/1505.00468>.
- [2] Shuai Bai, Keqin Chen, Xuejing Liu, Jialin Wang, Wenbin Ge, Sibao Song, Kai Dang, Peng Wang, Shijie Wang, Jun Tang, Humen Zhong, Yanzhi Zhu, Mingkun Yang, Zhaohai Li, Jianqiang Wan, Pengfei Wang, Wei Ding, Zheren Fu, Yiheng Xu, Jiabo Ye, Xi Zhang, Tianbao Xie, Zesen Cheng, Hang Zhang, Zhibo Yang, Haiyang Xu, and Junyang Lin. Qwen2.5-vl technical report, 2025. URL <https://arxiv.org/abs/2502.13923>.
- [3] Davide Caffagni, Federico Cocchi, Nicholas Moratelli, Sara Sarto, Marcella Cornia, Lorenzo Baraldi, and Rita Cucchiara. Wiki-llava: Hierarchical retrieval-augmented generation for multimodal llms, 2024. URL <https://arxiv.org/abs/2404.15406>.
- [4] Jun Chen, Deyao Zhu, Xiaoqian Shen, Xiang Li, Zechun Liu, Pengchuan Zhang, Raghuraman Krishnamoorthi, Vikas Chandra, Yunsang Xiong, and Mohamed Elhoseiny. Minigpt-v2: large language model as a unified interface for vision-language multi-task learning, 2023. URL <https://arxiv.org/abs/2310.09478>.
- [5] Wenhui Chen, Hexiang Hu, Xi Chen, Pat Verga, and William W. Cohen. Murag: Multimodal retrieval-augmented generator for open question answering over images and text, 2022. URL <https://arxiv.org/abs/2210.02928>.
- [6] Xi Chen, Josip Djolonga, Piotr Padlewski, Basil Mustafa, Soravit Changpinyo, Jialin Wu, Carlos Riquelme Ruiz, Sebastian Goodman, Xiao Wang, Yi Tay, Siamak Shakeri, Mostafa Dehghani, Daniel Salz, Mario Lucic, Michael Tschannen, Arsha Nagrai, Hexiang Hu, Mandar Joshi, Bo Pang, Ceslee Montgomery, Paulina Pietrzyk, Marvin Ritter, AJ Piergiovanni, Matthias Minderer, Filip Pavetic, Austin Waters, Gang Li, Ibrahim Alabdulmohsin, Lucas Beyer, Julien Amelot, Kenton Lee, Andreas Peter Steiner, Yang Li, Daniel Keysers, Anurag Arnab, Yanzhong Xu, Keran Rong, Alexander Kolesnikov, Mojtaba Seyedhosseini, Anelia Angelova, Xiaohua Zhai, Neil Houlsby, and Radu Soricut. Pali-x: On scaling up a multilingual vision and language model, 2023. URL <https://arxiv.org/abs/2305.18565>.
- [7] Zhe Chen, Jiannan Wu, Wenhui Wang, Weijie Su, Guo Chen, Sen Xing, Muyan Zhong, Qinglong Zhang, Xizhou Zhu, Lewei Lu, Bin Li, Ping Luo, Tong Lu, Yu Qiao, and Jifeng Dai. Internvl: Scaling up vision foundation models and aligning for generic visual-linguistic tasks, 2024. URL <https://arxiv.org/abs/2312.14238>.
- [8] Wei-Lin Chiang, Zhuohan Li, Zi Lin, Ying Sheng, Zhanghao Wu, Hao Zhang, Lianmin Zheng, Siyuan Zhuang, Yonghao Zhuang, Joseph E. Gonzalez, Ion Stoica, and Eric P. Xing. Vicuna: An open-source chatbot impressing gpt-4 with 90%* chatgpt quality, March 2023. URL <https://lmsys.org/blog/2023-03-30-vicuna/>.
- [9] Xiangxiang Chu, Limeng Qiao, Xinyang Lin, Shuang Xu, Yang Yang, Yiming Hu, Fei Wei, Xinyu Zhang, Bo Zhang, Xiaolin Wei, and Chunhua Shen. Mobilevlm : A fast, strong and open vision language assistant for mobile devices, 2023. URL <https://arxiv.org/abs/2312.16886>.
- [10] Xiangxiang Chu, Limeng Qiao, Xinyu Zhang, Shuang Xu, Fei Wei, Yang Yang, Xiaofei Sun, Yiming Hu, Xinyang Lin, Bo Zhang, and Chunhua Shen. Mobilevlm v2: Faster and stronger baseline for vision language model, 2024. URL <https://arxiv.org/abs/2402.03766>.
- [11] Chaoyou Fu, Peixian Chen, Yunhang Shen, Yulei Qin, Mengdan Zhang, Xu Lin, Jinrui Yang, Xiawu Zheng, Ke Li, Xing Sun, Yunsheng Wu, and Rongrong Ji. Mme: A comprehensive evaluation benchmark for multimodal large language models, 2024. URL <https://arxiv.org/abs/2306.13394>.
- [12] Google. Gemini 2.5 pro. <https://deepmind.google/technologies/gemini/>, 2024. Google DeepMind.

- [13] Suriya Gunasekar, Yi Zhang, Jyoti Aneja, Caio César Teodoro Mendes, Allie Del Giorno, Sivakanth Gopi, Mojan Javaheripi, Piero Kauffmann, Gustavo de Rosa, Olli Saarikivi, Adil Salim, Shital Shah, Harkirat Singh Behl, Xin Wang, Sébastien Bubeck, Ronen Eldan, Adam Tauman Kalai, Yin Tat Lee, and Yuanzhi Li. Textbooks are all you need, 2023. URL <https://arxiv.org/abs/2306.11644>.
- [14] Kelvin Guu, Kenton Lee, Zora Tung, Panupong Pasupat, and Ming-Wei Chang. Realm: Retrieval-augmented language model pre-training, 2020. URL <https://arxiv.org/abs/2002.08909>.
- [15] Ziniu Hu, Ahmet Iscen, Chen Sun, Zirui Wang, Kai-Wei Chang, Yizhou Sun, Cordelia Schmid, David A. Ross, and Alireza Fathi. Reveal: Retrieval-augmented visual-language pre-training with multi-source multimodal knowledge memory, 2023. URL <https://arxiv.org/abs/2212.05221>.
- [16] Drew A. Hudson and Christopher D. Manning. Gqa: A new dataset for real-world visual reasoning and compositional question answering, 2019. URL <https://arxiv.org/abs/1902.09506>.
- [17] Andrew Jaegle, Sebastian Borgeaud, Jean-Baptiste Alayrac, Carl Doersch, Catalin Ionescu, David Ding, Skanda Koppula, Daniel Zoran, Andrew Brock, Evan Shelhamer, Olivier Hénaff, Matthew M. Botvinick, Andrew Zisserman, Oriol Vinyals, and João Carreira. Perceiver io: A general architecture for structured inputs & outputs, 2022. URL <https://arxiv.org/abs/2107.14795>.
- [18] Ranjay Krishna, Yuke Zhu, Oliver Groth, Justin Johnson, Kenji Hata, Joshua Kravitz, Stephanie Chen, Yannis Kalantidis, Li-Jia Li, David A. Shamma, Michael S. Bernstein, and Fei-Fei Li. Visual genome: Connecting language and vision using crowdsourced dense image annotations, 2016. URL <https://arxiv.org/abs/1602.07332>.
- [19] Patrick Lewis, Ethan Perez, Aleksandra Piktus, Fabio Petroni, Vladimir Karpukhin, Naman Goyal, Heinrich Küttler, Mike Lewis, Wen tau Yih, Tim Rocktäschel, Sebastian Riedel, and Douwe Kiela. Retrieval-augmented generation for knowledge-intensive nlp tasks, 2021. URL <https://arxiv.org/abs/2005.11401>.
- [20] Junnan Li, Dongxu Li, Silvio Savarese, and Steven Hoi. Blip-2: Bootstrapping language-image pre-training with frozen image encoders and large language models, 2023. URL <https://arxiv.org/abs/2301.12597>.
- [21] Yifan Li, Yifan Du, Kun Zhou, Jinpeng Wang, Wayne Xin Zhao, and Ji-Rong Wen. Evaluating object hallucination in large vision-language models, 2023. URL <https://arxiv.org/abs/2305.10355>.
- [22] Tsung-Yi Lin, Michael Maire, Serge Belongie, Lubomir Bourdev, Ross Girshick, James Hays, Pietro Perona, Deva Ramanan, C. Lawrence Zitnick, and Piotr Dollár. Microsoft coco: Common objects in context, 2015. URL <https://arxiv.org/abs/1405.0312>.
- [23] Haotian Liu, Chunyuan Li, Qingyang Wu, and Yong Jae Lee. Visual instruction tuning, 2023. URL <https://arxiv.org/abs/2304.08485>.
- [24] Tianyu Liu, Jirui Qi, Paul He, Arianna Bisazza, Mrinmaya Sachan, and Ryan Cotterell. Point-wise mutual information as a performance gauge for retrieval-augmented generation, 2025. URL <https://arxiv.org/abs/2411.07773>.
- [25] Haoyu Lu, Wen Liu, Bo Zhang, Bingxuan Wang, Kai Dong, Bo Liu, Jingxiang Sun, Tongzheng Ren, Zhuoshu Li, Hao Yang, Yaofeng Sun, Chengqi Deng, Hanwei Xu, Zhenda Xie, and Chong Ruan. Deepseek-vl: Towards real-world vision-language understanding, 2024. URL <https://arxiv.org/abs/2403.05525>.
- [26] Pan Lu, Swaroop Mishra, Tony Xia, Liang Qiu, Kai-Wei Chang, Song-Chun Zhu, Oyvind Tafjord, Peter Clark, and Ashwin Kalyan. Learn to explain: Multimodal reasoning via thought chains for science question answering, 2022. URL <https://arxiv.org/abs/2209.09513>.

- [27] Andrés Marafioti, Orr Zohar, Miquel Farré, Merve Noyan, Elie Bakouch, Pedro Cuenca, Cyril Zakka, Loubna Ben Allal, Anton Lozhkov, Nouamane Tazi, Vaibhav Srivastav, Joshua Lochner, Hugo Larcher, Mathieu Morlon, Lewis Tunstall, Leandro von Werra, and Thomas Wolf. Smolvlm: Redefining small and efficient multimodal models, 2025. URL <https://arxiv.org/abs/2504.05299>.
- [28] Anand Mishra, Shashank Shekhar, Ajeet Kumar Singh, and Anirban Chakraborty. Ocr-vqa: Visual question answering by reading text in images. In *ICDAR*, 2019.
- [29] OpenAI. Gpt-4v(ision). <https://openai.com/research/gpt-4v-system-card>, 2023. OpenAI.
- [30] Alec Radford, Jong Wook Kim, Chris Hallacy, Aditya Ramesh, Gabriel Goh, Sandhini Agarwal, Girish Sastry, Amanda Askell, Pamela Mishkin, Jack Clark, Gretchen Krueger, and Ilya Sutskever. Learning transferable visual models from natural language supervision, 2021. URL <https://arxiv.org/abs/2103.00020>.
- [31] Varun Nagaraj Rao, Siddharth Choudhary, Aditya Deshpande, Ravi Kumar Satzoda, and Srikar Appalaraju. Raven: Multitask retrieval augmented vision-language learning, 2024. URL <https://arxiv.org/abs/2406.19150>.
- [32] Amanpreet Singh, Vivek Natarajan, Meet Shah, Yu Jiang, Xinlei Chen, Dhruv Batra, Devi Parikh, and Marcus Rohrbach. Towards vqa models that can read, 2019. URL <https://arxiv.org/abs/1904.08920>.
- [33] Andreas Steiner, André Susano Pinto, Michael Tschannen, Daniel Keysers, Xiao Wang, Yonatan Bitton, Alexey Gritsenko, Matthias Minderer, Anthony Sherbondy, Shangbang Long, Siyang Qin, Reeve Ingle, Emanuele Bugliarello, Sahar Kazemzadeh, Thomas Mesnard, Ibrahim Al-abdulmohsin, Lucas Beyer, and Xiaohua Zhai. Paligemma 2: A family of versatile vlms for transfer, 2024. URL <https://arxiv.org/abs/2412.03555>.
- [34] Gemma Team, Morgane Riviere, Shreya Pathak, Pier Giuseppe Sessa, Cassidy Hardin, Surya Bhupatiraju, Léonard Hussenot, Thomas Mesnard, Bobak Shahriari, Alexandre Ramé, Johan Ferret, Peter Liu, Pouya Tafti, Abe Friesen, Michelle Casbon, Sabela Ramos, Ravin Kumar, Charline Le Lan, Sammy Jerome, Anton Tsitsulin, Nino Vieillard, Piotr Stanczyk, Sertan Girgin, Nikola Momchev, Matt Hoffman, Shantanu Thakoor, Jean-Bastien Grill, Behnam Neyshabur, Olivier Bachem, Alanna Walton, Aliaksei Severyn, Alicia Parrish, Aliya Ahmad, Allen Hutchison, Alvin Abdagic, Amanda Carl, Amy Shen, Andy Brock, Andy Coenen, Anthony Laforge, Antonia Paterson, Ben Bastian, Bilal Piot, Bo Wu, Brandon Royal, Charlie Chen, Chintu Kumar, Chris Perry, Chris Welty, Christopher A. Choquette-Choo, Danila Sinopalnikov, David Weinberger, Dimple Vijaykumar, Dominika Rogozińska, Dustin Herbison, Elisa Bandy, Emma Wang, Eric Noland, Erica Moreira, Evan Senter, Evgenii Eltyshov, Francesco Visin, Gabriel Rasskin, Gary Wei, Glenn Cameron, Gus Martins, Hadi Hashemi, Hanna Klimczak-Plucińska, Harleen Batra, Harsh Dhand, Ivan Nardini, Jacinda Mein, Jack Zhou, James Svensson, Jeff Stanway, Jetha Chan, Jin Peng Zhou, Joana Carrasqueira, Joana Iljazi, Jocelyn Becker, Joe Fernandez, Joost van Amersfoort, Josh Gordon, Josh Lipschultz, Josh Newlan, Ju yeong Ji, Kareem Mohamed, Kartikeya Badola, Kat Black, Katie Millican, Keelin McDonell, Kelvin Nguyen, Kiranbir Sodhia, Kish Greene, Lars Lowe Sjoesund, Lauren Usui, Laurent Sifre, Lena Heuermann, Leticia Lago, Lilly McNealus, Livio Baldini Soares, Logan Kilpatrick, Lucas Dixon, Luciano Martins, Machel Reid, Manvinder Singh, Mark Iverson, Martin Görner, Mat Velloso, Mateo Wirth, Matt Davidow, Matt Miller, Matthew Rahtz, Matthew Watson, Meg Risdal, Mehran Kazemi, Michael Moynihan, Ming Zhang, Minsuk Kahng, Minwoo Park, Mofi Rahman, Mohit Khatwani, Natalie Dao, Nenshad Bardoliwalla, Nesh Devanathan, Neta Dumai, Nilay Chauhan, Oscar Wahltinez, Pankil Botarda, Parker Barnes, Paul Barham, Paul Michel, Pengchong Jin, Petko Georgiev, Phil Culliton, Pradeep Kuppala, Ramona Comanescu, Ramona Merhej, Reena Jana, Reza Ardeshtir Rokni, Rishabh Agarwal, Ryan Mullins, Samaneh Saadat, Sara Mc Carthy, Sarah Cogan, Sarah Perrin, Sébastien M. R. Arnold, Sebastian Krause, Shengyang Dai, Shruti Garg, Shruti Sheth, Sue Ronstrom, Susan Chan, Timothy Jordan, Ting Yu, Tom Eccles, Tom Hennigan, Tomas Kocisky, Tulsee Doshi, Vihan Jain, Vikas Yadav, Vilobh Meshram, Vishal Dharmadhikari, Warren Barkley, Wei Wei, Wenming Ye, Woohyun Han, Woosuk Kwon, Xiang Xu, Zhe Shen, Zhitao Gong, Zichuan Wei, Victor Cotruta, Phoebe

- Kirk, Anand Rao, Minh Giang, Ludovic Peran, Tris Warkentin, Eli Collins, Joelle Barral, Zoubin Ghahramani, Raia Hadsell, D. Sculley, Jeanine Banks, Anca Dragan, Slav Petrov, Oriol Vinyals, Jeff Dean, Demis Hassabis, Koray Kavukcuoglu, Clement Farabet, Elena Buchatskaya, Sebastian Borgeaud, Noah Fiedel, Armand Joulin, Kathleen Kenealy, Robert Dadashi, and Alek Andrejev. Gemma 2: Improving open language models at a practical size, 2024. URL <https://arxiv.org/abs/2408.00118>.
- [35] Tiannan Wang, Wangchunshu Zhou, Yan Zeng, and Xinsong Zhang. Efficientvlm: Fast and accurate vision-language models via knowledge distillation and modal-adaptive pruning. *arXiv preprint arXiv:2210.07795*, 2022.
- [36] An Yang, Baosong Yang, Binyuan Hui, Bo Zheng, Bowen Yu, Chang Zhou, Chengpeng Li, Chengyuan Li, Dayiheng Liu, Fei Huang, Guanting Dong, Haoran Wei, Huan Lin, Jialong Tang, Jialin Wang, Jian Yang, Jianhong Tu, Jianwei Zhang, Jianxin Ma, Jianxin Yang, Jin Xu, Jingren Zhou, Jinze Bai, Jinzheng He, Junyang Lin, Kai Dang, Keming Lu, Keqin Chen, Kexin Yang, Mei Li, Mingfeng Xue, Na Ni, Pei Zhang, Peng Wang, Ru Peng, Rui Men, Ruize Gao, Runji Lin, Shijie Wang, Shuai Bai, Sinan Tan, Tianhang Zhu, Tianhao Li, Tianyu Liu, Wenbin Ge, Xiaodong Deng, Xiaohuan Zhou, Xingzhang Ren, Xinyu Zhang, Xipin Wei, Xuancheng Ren, Xuejing Liu, Yang Fan, Yang Yao, Yichang Zhang, Yu Wan, Yunfei Chu, Yuqiong Liu, Zeyu Cui, Zhenru Zhang, Zhifang Guo, and Zhihao Fan. Qwen2 technical report, 2024. URL <https://arxiv.org/abs/2407.10671>.
- [37] Zhengyuan Yang, Linjie Li, Jianfeng Wang, Kevin Lin, Ehsan Azarnasab, Faisal Ahmed, Zicheng Liu, Ce Liu, Michael Zeng, and Lijuan Wang. Mm-react: Prompting chatgpt for multimodal reasoning and action, 2023. URL <https://arxiv.org/abs/2303.11381>.
- [38] Zhuolin Yang, Wei Ping, Zihan Liu, Vijay Korthikanti, Weili Nie, De-An Huang, Linxi Fan, Zhiding Yu, Shiyi Lan, Bo Li, Ming-Yu Liu, Yuke Zhu, Mohammad Shoeybi, Bryan Catanzaro, Chaowei Xiao, and Anima Anandkumar. Re-vilm: Retrieval-augmented visual language model for zero and few-shot image captioning, 2023. URL <https://arxiv.org/abs/2302.04858>.
- [39] Yuan Yao, Tianyu Yu, Ao Zhang, Chongyi Wang, Junbo Cui, Hongji Zhu, Tianchi Cai, Haoyu Li, Weilin Zhao, Zhihui He, Qianyu Chen, Huarong Zhou, Zhensheng Zou, Haoye Zhang, Shengding Hu, Zhi Zheng, Jie Zhou, Jie Cai, Xu Han, Guoyang Zeng, Dahai Li, Zhiyuan Liu, and Maosong Sun. Minicpm-v: A gpt-4v level mllm on your phone, 2024. URL <https://arxiv.org/abs/2408.01800>.
- [40] Weihao Yu, Zhengyuan Yang, Linjie Li, Jianfeng Wang, Kevin Lin, Zicheng Liu, Xinchao Wang, and Lijuan Wang. Mm-vet: Evaluating large multimodal models for integrated capabilities, 2024. URL <https://arxiv.org/abs/2308.02490>.
- [41] Zhengqing Yuan, Zhaoxu Li, Weiran Huang, Yanfang Ye, and Lichao Sun. Tinygpt-v: Efficient multimodal large language model via small backbones, 2024. URL <https://arxiv.org/abs/2312.16862>.
- [42] Xiang Yue, Yuansheng Ni, Kai Zhang, Tianyu Zheng, Ruoqi Liu, Ge Zhang, Samuel Stevens, Dongfu Jiang, Weiming Ren, Yuxuan Sun, Cong Wei, Botao Yu, Ruibin Yuan, Renliang Sun, Ming Yin, Boyuan Zheng, Zhenzhu Yang, Yibo Liu, Wenhao Huang, Huan Sun, Yu Su, and Wenhua Chen. Mmmu: A massive multi-discipline multimodal understanding and reasoning benchmark for expert agi, 2024. URL <https://arxiv.org/abs/2311.16502>.
- [43] Xiaohua Zhai, Basil Mustafa, Alexander Kolesnikov, and Lucas Beyer. Sigmoid loss for language image pre-training, 2023. URL <https://arxiv.org/abs/2303.15343>.
- [44] Peiyuan Zhang, Guangtao Zeng, Tianduo Wang, and Wei Lu. Tinyllama: An open-source small language model, 2024. URL <https://arxiv.org/abs/2401.02385>.
- [45] Baichuan Zhou, Ying Hu, Xi Weng, Junlong Jia, Jie Luo, Xien Liu, Ji Wu, and Lei Huang. Tinyllava: A framework of small-scale large multimodal models, 2024. URL <https://arxiv.org/abs/2402.14289>.
- [46] Deyao Zhu, Jun Chen, Xiaoqian Shen, Xiang Li, and Mohamed Elhoseiny. Minigpt-4: Enhancing vision-language understanding with advanced large language models, 2023. URL <https://arxiv.org/abs/2304.10592>.

- [47] Kun Zhu, Xiaocheng Feng, Xiyuan Du, Yuxuan Gu, Weijiang Yu, Haotian Wang, Qianglong Chen, Zheng Chu, Jingchang Chen, and Bing Qin. An information bottleneck perspective for effective noise filtering on retrieval-augmented generation, 2024. URL <https://arxiv.org/abs/2406.01549>.

A Detailed Analysis on Enhancing Effective Mutual Information via RAG

As discussed, Lightweight, frozen LLMs ($\theta_{\text{LLM,small}}$) often exhibit performance limitations due to a substantial irreducible error $\bar{\epsilon}_{\theta_{\text{LLM}}}$. To mitigate this, we introduce TinyAlign (Fig. 1), a Retrieval-Augmented Generation (RAG)-enhanced connector architecture. This approach boosts *effective mutual information* (I_{eff}) by supplying strategically compressed, highly relevant contextual cues, thereby reducing the intrinsic processing demands on the frozen LLM.

A standard VLM processes a visual input X_V via a ViT (θ_{ViT}) to obtain Z_V , which a primary connector (θ_C^*) maps to H_V . Instruction embeddings H_I are also generated. TinyAlign augments this by: 1) retrieving k relevant, pre-compressed embeddings $E_R = \{E_{R_j}\}_{j=1}^k$ from a memory bank \mathcal{M} (Sec. 4.2); 2) employing a trainable RAG connector (θ_{RC}^*) to transform E_R into supplementary representations H_R ; and 3) presenting a composite input $H_{\text{in}}' = [H_V, H_R, H_I]$ to the frozen LLM. The trainable parameters are thus $\Theta_C^* = \{\theta_C^*, \theta_{RC}^*\}$. We posit that incorporating E_R —forming an augmented context $X' = (X_V, X_I, E_R)$ —enhances $I_{\text{eff}}(X'; L | \theta_{\text{LLM}}, \theta_{\text{ViT}})$. The change, ΔI_{eff} , is:

$$\begin{aligned} \Delta I_{\text{eff}} &= [I(X'; L) - \bar{\epsilon}_{\theta_{\text{LLM}}}(X')] - [I(X_V, X_I; L) - \bar{\epsilon}_{\theta_{\text{LLM}}}(X_V, X_I)] \\ &= \underbrace{I(E_R; L | X_V, X_I)}_{\Delta I_{\text{true}}} + \underbrace{(\bar{\epsilon}_{\theta_{\text{LLM}}}(X_V, X_I) - \bar{\epsilon}_{\theta_{\text{LLM}}}(X'))}_{\Delta \bar{\epsilon}_{\theta_{\text{LLM}}}} \end{aligned} \quad (7)$$

The first term, ΔI_{true} , is positive because E_R , derived from pertinent captions (i.e., clues for the target L), provides novel information about L conditioned on X_V and X_I . The second term, $\Delta \bar{\epsilon}_{\theta_{\text{LLM}}}$, signifies a positive reduction in the LLM’s irreducible error. The RAG connector θ_{RC}^* transforms E_R into H_R , providing what we term ‘concise, LLM-assimilable contextual hints.’ These hints—originating from pre-compressed image-text pairs (potent clues processed by θ_P)—present information in a format more attuned to the LLM’s textual processing strengths than deciphering complex visual semantics solely from H_V . This enhanced ‘input friendliness’ of the augmented input H_{in}' enables the fixed-capacity LLM to approximate the target distribution $P_{\text{true}}(L | X')$ with greater fidelity than it could from (X_V, X_I) alone, a phenomenon corroborated by faster convergence (Fig. 2(a)). This improved fidelity directly translates into fewer fundamental misinterpretations, thereby lowering the irreducible error: $\bar{\epsilon}_{\theta_{\text{LLM}}}(X') < \bar{\epsilon}_{\theta_{\text{LLM}}}(X_V, X_I)$. The trainable RAG connector θ_{RC}^* is optimized to generate H_R that maximizes this error reduction by effectively complementing H_V and H_I , thus alleviating the LLM’s cognitive burden.

This reduction in irreducible error is especially impactful for lightweight VLMs, whose inherent capacity constraints often yield a higher baseline $\bar{\epsilon}_{\theta_{\text{LLM}}}(X_V, X_I)$. TinyAlign’s architecture—emphasizing LLM-independent, Perceiver-based pre-compression for the memory bank and an efficient RAG connector—is engineered to maximize this $\Delta \bar{\epsilon}_{\theta_{\text{LLM}}}$. It functions as a ‘cognitive scaffold,’ substantially lowering the reasoning threshold for these less capable LLMs—a benefit less critical for LLMs endowed with robust intrinsic reasoning. Consequently, when $\Delta I_{\text{eff}} > 0$ —driven by both $\Delta I_{\text{true}} > 0$ and a substantial $\Delta \bar{\epsilon}_{\theta_{\text{LLM}}} > 0$ for lightweight LLMs—the system’s minimum achievable CE loss is reduced: $\min_{\theta_C^*} \mathcal{L}_{\text{CE}}(\text{RAG-enhanced}) < \min_{\theta_C^*} \mathcal{L}_{\text{CE}}(\text{standard})$. This framework demonstrates that RAG-enhanced connectors, by strategically mitigating the processing burden and inherent error of a frozen (especially lightweight) LLM using pre-compressed multimodal cues, can elevate VLM performance. This effectively increases the information the LLM can leverage despite its fixed capacity.

B Hyperparameter Summary

This subsection provides a comprehensive overview of the critical hyperparameters employed throughout our experimental phases, encompassing both pre-training and fine-tuning stages for our proposed models, as well as the specific configuration for the Perceiver model utilized in TinyAlign’s memory bank construction. Table 2 delineates the comparative settings for pre-training and fine-tuning, covering aspects such as batch sizes, learning rates, and optimization strategies. Complementing this, Table 3 itemizes the architectural hyperparameters of the Perceiver model, detailing its latent space dimensions, attention mechanisms, and input specifications. All experiments were conducted on a system equipped with eight NVIDIA RTX 4090 GPUs, each with 48GB of VRAM, ensuring robust and scalable computational support.

Table 2: Key hyperparameters for pre-training and fine-tuning.

Hyperparameter	Pre-training Value	Fine-tuning Value
Global Batch Size	256	128
Per-device Batch Size (script)	16	12
Gradient Accumulation (script)	1	2
Learning Rate	1e-3	5e-8
LR Scheduler	Cosine	Cosine
Warmup Ratio	0.03	0.03
Precision	FP16	FP16
Optimizer	AdamW	AdamW
LLM Tuning	Frozen	Full
Vision Tower Tuning	Frozen	Frozen
Connector Tuning	Full	Full

Table 3: PerceiverConfig Hyperparameters

Parameter	Value
num_latents	32
d_latents	96
d_model	128
num_self_attends_per_block	8
num_blocks	1
num_self_attention_heads	8
num_cross_attention_heads	8
qk_channels	96
v_channels	96
image_size	384
vocab_size	30522
max_position_embeddings	512

C UMAP Visualization of Feature Embeddings

To elucidate the latent structure and interrelations between image-derived and text-derived features, we employed Uniform Manifold Approximation and Projection (UMAP) for dimensionality reduction and visualization.

UMAP Fundamentals: UMAP is a non-linear dimensionality reduction algorithm adept at preserving both local and global structures of high-dimensional data within a lower-dimensional embedding. It achieves this by first constructing a high-dimensional graph representation of the data, where edge weights denote the likelihood of connectivity between points. Subsequently, it optimizes a low-dimensional graph to maximize structural similarity to its high-dimensional counterpart. This methodology is rooted in Riemannian geometry and algebraic topology, aiming to model the data’s underlying manifold.

Visualization Methodology: Our UMAP-based visualization procedure comprised the following steps:

1. **Input Data Preparation:** The UMAP process utilized two sets of high-dimensional feature vectors:
 - **Connector Features:** Vectors derived from images post-processing by the vision tower and the model’s connector module. These represent visual information conditioned for the language model.
 - **LLM Input Embeddings:** Corresponding vectors representing embeddings of textual inputs (e.g., questions, prompts) from the language model’s input embedding layer.

These two feature sets were concatenated. Origin labels (connector feature or LLM embedding) were retained for subsequent differentiated visualization.

2. **UMAP Dimensionality Reduction:** The UMAP algorithm was applied to the concatenated high-dimensional dataset, configured to reduce feature dimensionality to two. This 2D representation facilitates direct scatter plot visualization. The algorithm learns a mapping that optimally preserves the topological structure of the original feature space in this lower dimension.
3. **Output and Visualization:** The UMAP process yielded:
 - **2D Coordinates:** A two-dimensional coordinate (x, y) for each input feature vector (both connector and LLM embedding).
 - **Scatter Plot Visualization:** These 2D coordinates were used to generate a scatter plot. Points corresponding to connector features and LLM input embeddings were rendered in distinct colors. This visualization enables qualitative assessment of:
 - The distinctness or overlap between the two feature spaces.
 - The presence of intra-feature-type clusters.
 - The overall geometric relationship between the model’s latent representations of visual and textual information.

D FLOPs Analysis

This section presents a comparative analysis of the Floating Point Operations (FLOPs) for models based on the Phi-2 architecture, focusing on the computational demands during different stages. As detailed in Table 4, we evaluate both our proposed TinyAlign approach and a baseline model across pre-training and fine-tuning phases. The analysis indicates that while the introduction of RAG tokens and an additional RAG connector in TinyAlign incurs a marginal increase in computational operations, the overall impact on inference efficiency and training throughput remains negligible, underscoring the computational viability of our method.

Table 4: FLOPs analysis for Phi-2 based models. While the introduction of RAG tokens and an additional RAG connector incurs a marginal increase in computational operations, the impact on overall inference efficiency is negligible.

Model Stage	Train Steps/Second	FLOPs
TinyAlign-finetune	0.075	6.15e18
TinyAlign-pretrain	0.112	2.45e14
Baseline-finetune	0.083	6.12e18
Baseline-pretrain	0.173	2.05e14

E Detailed Data Efficiency Analysis

TinyAlign models exhibit remarkable data efficiency during instruction tuning, as illustrated comparatively in Fig. 3 (main text) and further detailed per benchmark in Fig. 4. Our comprehensive analysis indicates that TinyAlign-enhanced models, specifically LightweightLLM-Phi-2 and TinyLLaMA, can match the weighted average accuracy of baseline models trained with 100% of the instruction tuning data while using only 40% of this data. A granular examination of individual benchmarks further substantiates TinyAlign’s effectiveness in learning from limited labeled data and enhancing critical VLM capabilities.

Enhanced Visual Reasoning with Greater Efficiency. On visual reasoning benchmarks, TinyAlign yields substantial data efficiency gains. For **GQA**, TinyAlign (SigLIP-384-phi-2, 2.7B) with 60% data (59.7 accuracy) surpasses the baseline with 100% data (58.4 accuracy). Similarly, TinyAlign (SigLIP-384-TinyLlama, 1.1B) with just 40% data (52.78 accuracy) outperforms its baseline counterpart using 100% data (52.37 accuracy). On **VQAv2**, TinyAlign (SigLIP-384-phi-2, 2.7B) at 40% data (75.64 accuracy) matches the baseline’s full-data performance (75.39 accuracy), while TinyAlign (SigLIP-384-TinyLlama, 1.1B) with 40% data (72.50 accuracy) significantly exceeds its baseline with 100% data (70.98 accuracy). For **SQA-I**, the TinyAlign-enhanced TinyLlama model demonstrates a particularly notable improvement in its performance trajectory with increasing data efficiency, compared to a relatively stagnant baseline.

Improved Scene Text Understanding. TinyAlign’s advantages extend to scene text understanding. On **TextVQA**, TinyAlign (SigLIP-384-phi-2, 2.7B) utilizing only 40% of the training data (51.10 accuracy) achieves higher accuracy than the baseline model trained with 100% data (50.31 accuracy), suggesting an improved ability to integrate visual and textual cues from sparser signals.

Effective Suppression of Model Hallucinations. TinyAlign significantly enhances model factuality by reducing hallucinations, as evidenced on the **POPE** benchmark. TinyAlign models consistently achieve higher accuracy (implying fewer hallucinations) across various data proportions. For instance, TinyAlign (SigLIP-384-TinyLlama, 1.1B) with only 20% data (85.6 accuracy) surpasses the baseline TinyLlama trained with 100% data (84.3 accuracy). TinyAlign (SigLIP-384-phi-2, 2.7B) exhibits similar data efficiency, reaching the baseline’s peak performance with only 40% of the data.

Broad Applicability and Efficacy on Lightweight Models. On comprehensive benchmarks such as **MME**, TinyAlign generally provides consistent performance improvements for both Phi-2 and TinyLlama backbones. For instance, TinyAlign-enhanced models show a clear advantage over baselines across most data regimes on MME. On **MM-Vet**, data efficiency is also prominent: TinyAlign (SigLIP-384-phi-2, 2.7B) with 20% data (32.2 accuracy) outperforms the baseline with 100% data (31.5 accuracy), while TinyAlign (SigLIP-384-TinyLlama, 1.1B) with 40% data (24.6 accuracy) performs comparably to its baseline with 100% data (24.8 accuracy).

Addressing Challenges in Complex Tasks. While TinyAlign demonstrates broad advantages, its impact can vary with task complexity. On the highly intricate **MMM** benchmark, performance gains from TinyAlign are less consistent across data proportions compared to other benchmarks. Furthermore, on **MM-Vet**, the baseline TinyLlama model slightly outperforms its TinyAlign counterpart when both are trained with 100% data. These instances suggest avenues for future research, such as optimizing TinyAlign for extremely complex tasks or specific model-data interactions.

To comprehensively evaluate the model’s overall performance across multiple distinct benchmark datasets, we employed **weighted average accuracy**. This method assigns a corresponding weight based on the sample size (or representative importance) C_i of each test set. For the accuracies Acc_i obtained for each test set under specific conditions (e.g., a certain training data percentage), the weighted average accuracy A_{weighted} is calculated as follows:

$$A_{\text{weighted}} = \frac{\sum (Acc_i \times C_i)}{\sum C_i} \quad (8)$$

This approach allows us to more accurately reflect the model’s combined performance on datasets of varying scales and characteristics, avoiding potential biases from simple averaging.

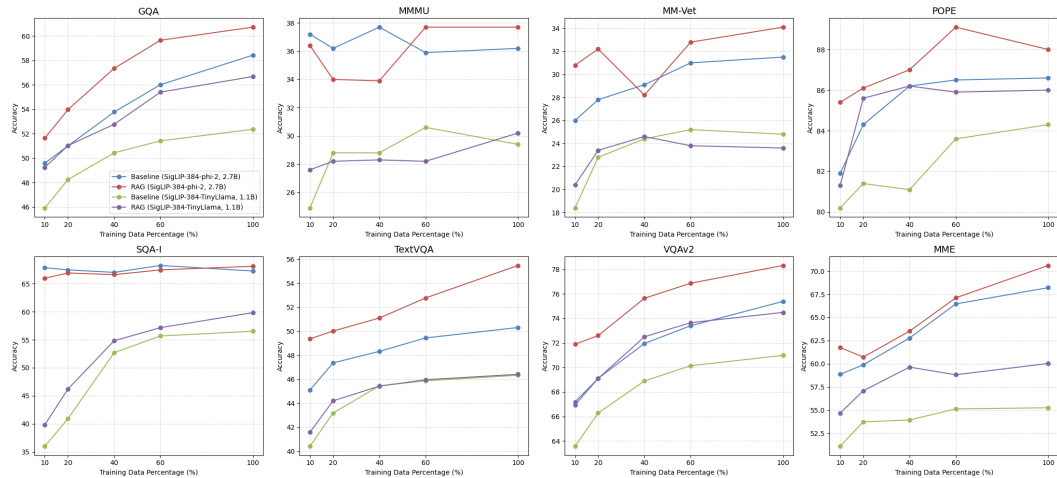


Figure 4: Detailed data efficiency analysis across individual benchmarks. Performance of TinyAlign-enhanced models (variants of Phi-2 and TinyLLaMA) is compared against their respective baselines at varying percentages of instruction tuning data.

F Detailed Ablation Studies

We conduct several ablation studies to validate key design choices within the TinyAlign framework. These studies focus on knowledge base (KB) size, vision encoder alignment for RAG key generation, and the number of retrieved documents (Top-K). All ablations use the Phi-2 (2.7B) model as the LLM backbone unless otherwise specified.

Knowledge Base Size. We evaluate KB sizes of 100k, 300k, and 500k entries, with retrieval fixed at top-10 documents (Table 5). The 100k KB shows comparable, and in some cases superior, performance to larger KBs while offering greater efficiency. This finding suggests that a moderately sized, high-quality KB is sufficient and eliminates the need for excessively large memory banks.

Table 5: Ablation on knowledge base (KB) size for Phi-2 (2.7B) with top-10 retrieval. Performance reported on various benchmarks.

KB Size	GQA	MMMU	MM-Vet	POPE	SQA-I	TextVQA	VQAv2	MME
100k	60.73	37.7	34.1	0.880	68.12	55.48	78.32	1412.1
300k	61.27	36.8	31.7	0.871	70.25	55.42	78.58	1407.34
500k	61.38	36.0	31.6	0.875	68.91	56.43	78.57	1401.06

Vision Encoder Alignment for RAG Keys. We investigate the importance of aligning the vision encoder used for VLM pre-training with the encoder used for generating RAG keys (Table 6). Using `stablelm-2-zephyr-1.6b` as the VLM, we compare a matched configuration (VLM pre-trained with SigLIP features, RAG keys from SigLIP) against a baseline VLM (pre-trained with CLIP features, no RAG) and a mismatched RAG configuration (VLM pre-trained with CLIP features, RAG keys from SigLIP). The results show significant performance degradation, including a "collapse" on benchmarks like VQAv2, when encoders are mismatched. This highlights the critical importance of feature space consistency between the VLM’s learned representations and the RAG system’s retrieval mechanism. The "TinyAlign (Matched)" configuration, representing our proposed approach, consistently performs on par with or better than the CLIP VLM baseline, demonstrating the advantages of properly aligned RAG systems.

Table 6: Ablation on vision encoder alignment. VLM: `stablelm-2-zephyr-1.6b`. KB: 100k SigLIP-keyed. "Matched": VLM (SigLIP features) + RAG (SigLIP keys). "Baseline": VLM (CLIP features), no RAG. "Mismatched": VLM (CLIP features) + RAG (SigLIP keys).

Benchmark	TinyAlign (Matched: SigLIP VLM + SigLIP RAG)	Baseline (CLIP VLM)	TinyAlign (Mismatched: CLIP VLM + SigLIP RAG)
GQA	51.28	52.73	40.96
MMMU	0.304	0.313	0.300
MM-Vet	28.4	28.4	24.6
POPE	0.847	0.836	0.783
SQA-I	62.32	62.47	56.17
TextVQA	49.39	46.75	36.71
VQAv2	70.12	69.82	29.62
MME	1218.40	1206.49	1054.78

Table 7: Ablation on top-K retrieval for Phi-2 (2.7B) with a 100k knowledge base.

Top-K	GQA	MMMU	MM-Vet	POPE	SQA-I	TextVQA	VQAv2	MME
Top-1	60.6	36.0	33.2	0.874	70.35	55.66	78.21	1411.12
Top-5	61.27	38.1	33.6	0.874	70.00	55.69	78.48	1415.22
Top-10	60.73	37.7	34.1	0.880	68.12	55.48	78.32	1412.1

Top-K Retrieval. Using the 100k KB, we ablate the number of retrieved documents (Top-K) for Phi-2, comparing top-1, top-5, and top-10 retrieval (Table 7). Retrieving the top-5 documents achieves the best overall balance of performance across benchmarks, providing richer contextual signals than top-1 while avoiding the potential noise or diminishing returns observed with top-10 in some cases.